

# Lawrence Berkeley National Laboratory

## LBL Publications

### Title

Performances of a large mass ZnMoO<sub>4</sub> scintillating bolometer for a next generation 0vDBD experiment

### Permalink

<https://escholarship.org/uc/item/18d4x1rc>

### Journal

European Physical Journal C, 72(9)

### ISSN

1434-6044

### Authors

Beeman, JW  
Bellini, F  
Brofferio, C  
[et al.](#)

### Publication Date

2012-09-01

### DOI

10.1140/epjc/s10052-012-2142-7

Peer reviewed

# Performances of a large mass $\text{ZnMoO}_4$ scintillating bolometer for a next generation $0\nu\text{DBD}$ experiment

J.W. Beeman<sup>1</sup>, F. Bellini<sup>2,3</sup>, C. Brofferio<sup>4,5</sup>, L. Cardani<sup>2,3</sup>, N. Casali<sup>6,7</sup>, O. Cremonesi<sup>5</sup>, I. Dafinei<sup>3</sup>, S. Di Domizio<sup>8</sup>, F. Ferroni<sup>2,3</sup>, E. Gorello<sup>2,3</sup>, E.N. Galashov<sup>9</sup>, L. Gironi<sup>4,5</sup>, S.S. Nagorny<sup>10</sup>, F. Orio<sup>3</sup>, M. Pavan<sup>4,5</sup>, L. Pattavina<sup>5</sup>, G. Pessina<sup>5</sup>, G. Piperno<sup>2,3</sup>, S. Pirro<sup>5,a</sup>, E. Previtali<sup>5</sup>, C. Rusconi<sup>5</sup>, V.N. Shlegel<sup>9</sup>, C. Tomei<sup>3</sup>, M. Vignati<sup>3</sup>

<sup>1</sup>Lawrence Berkeley National Laboratory, Berkeley, CA 94720, USA

<sup>2</sup>Dipartimento di Fisica, Sapienza Università di Roma, 00185 Rome, Italy

<sup>3</sup>Sezione di Roma, INFN, 00185 Rome, Italy

<sup>4</sup>Dipartimento di Fisica, Università di Milano-Bicocca, 20126 Milano, Italy

<sup>5</sup>Sezione di Milano Bicocca, INFN, 20126 Milano, Italy

<sup>6</sup>Dipartimento di Fisica, Università degli studi dell'Aquila, 67100 L'Aquila, Italy

<sup>7</sup>Laboratori Nazionali del Gran Sasso, INFN, 67010 L'Aquila, Italy

<sup>8</sup>Sezione di Genova, INFN, 16146 Genova, Italy

<sup>9</sup>Nikolaev Institute of Inorganic Chemistry - SB RAS, 630090 Novosibirsk, Russia

<sup>10</sup>Institute for Nuclear Research, 03680 Kyiv, Ukraine

Received: 5 July 2012

© The Author(s) 2012. This article is published with open access at Springerlink.com

**Abstract** We present the performances of a 330 g zinc molybdate ( $\text{ZnMoO}_4$ ) crystal working as scintillating bolometer as a possible candidate for a next generation experiment to search for neutrinoless double beta decay of  $^{100}\text{Mo}$ . The energy resolution, evaluated at the 2615 keV  $\gamma$ -line of  $^{208}\text{Tl}$ , is 6.3 keV FWHM. The internal radioactive contaminations of the  $\text{ZnMoO}_4$  were evaluated as  $<6 \mu\text{Bq/kg}$  ( $^{228}\text{Th}$ ) and  $27 \pm 6 \mu\text{Bq/kg}$  ( $^{226}\text{Ra}$ ). We also present the results of the  $\alpha$  vs  $\beta/\gamma$  discrimination, obtained through the scintillation light as well as through the study of the shape of the thermal signal alone.

## 1 Introduction

The neutrinoless Double Beta Decay ( $0\nu\text{DBD}$ ) is a nuclear process that, if observed, would establish that the total lepton number is not a conserved quantity and that the neutrino is a Majorana particle, and would set the absolute mass scale of neutrinos [1–3]. Plenty of experiments are now in the construction phase and many others are in R&D phase [4]. Very recently EXO [5] and KamLAND-Zen [6] set very competitive limits on the  $0\nu\text{DBD}$  half-life of  $^{136}\text{Xe}$ .

The main challenges for all the different experimental techniques are the same [7]: (i) increase of the active mass, (ii) decrease of the background, and (iii) improvement of the energy resolution.

Thermal bolometers are ideal detectors for this kind of research: crystals can be grown with a variety of interesting DBD-emitters and multi-kg detectors can be operated with excellent energy resolution [8] which, perhaps, represents one of the most critical aspects for next generation experiments.

The Cuoricino experiment [9] searched for the  $0\nu\text{DBD}$  of  $^{130}\text{Te}$  operating 62  $\text{TeO}_2$  bolometers. The Cuoricino data demonstrated that the background in the region of interest is dominated by radioactive contaminations on the surfaces facing the detectors.  $\alpha$  particles produced by these contaminants can lose a fraction of their energy in the host material, and the rest in the detector, thus producing a flat background from the energy of the decay (several MeV) down to the  $0\nu\text{DBD}$  region [10]. Moreover simulations show that this contribution will largely dominate the expected background of the CUORE experiment [11, 12] in the region of interest, since  $\text{TeO}_2$  bolometers do not allow to distinguish  $\alpha$  particles from the electrons emitted in the  $0\nu\text{DBD}$ .

The natural way to discriminate this background, is to use scintillating bolometers [13]. In such devices the simultaneous and independent readout of the heat and the scintillation light signals permits to discriminate events due to  $\beta/\gamma$ ,  $\alpha$  and neutrons interactions thanks to their different scintillation yield.

$^{100}\text{Mo}$  is a very interesting  $\beta\beta$ -isotope because of its large transition energy  $Q_{\beta\beta} = 3034 \text{ keV}$  and a considerable natural isotopic abundance  $\delta = 9.67 \%$ . Several inorganic scintillators containing molybdenum were developed in the

<sup>a</sup>e-mail: [Stefano.pirro@mib.infn.it](mailto:Stefano.pirro@mib.infn.it)

last years. Among them,  $\text{ZnMoO}_4$  was recently grown [14] and the first cryogenic detector gave very promising results [15]. Some scintillating crystals, the molybdates in particular, show a very peculiar feature: the thermal pulse induced by an  $\alpha$  particle shows a slightly faster decay time with respect to the one induced by  $\gamma$  interactions [16]. This feature seems to be explained [17] by the relatively long scintillation decay time (of the order of hundreds of  $\mu\text{s}$ ) observed in some scintillating crystals. This long decay, combined with a high percentage of non-radiative de-excitation of the scintillation channel, will transfer phonons (i.e. heat) to the crystal. This extremely tiny, but measurable, time dependent phonon release has a different absolute value for isoenergetic  $\alpha$  and  $\beta/\gamma$  particles due to their different scintillation yield.

It was very recently measured that the  $\alpha$  vs  $\gamma$  separation on a 29 g  $\text{ZnMoO}_4$  crystal can reach an extremely high efficiency [19] using the pulse shape discrimination (PSD) alone, while the separation based on the scintillation light, even on smaller crystals (5 g), shows a smaller efficiency [20].

A next generation experiment, nonetheless, will need to run detectors with a considerably larger mass (of the order of few hundreds of grams each). It is not straightforward to foresee the performance of the particle discrimination method over a significantly larger sample. This is due to the fact that the PSD is sensitive to the signal to noise ratio, and a larger mass of the absorber crystal leads to a smaller signal amplitude ( $\propto (\text{detector mass})^{-1}$ ). The same holds (in principle) for the discrimination based on the scintillation light: usually (especially in the case of non transparent crystals) the larger the crystal, the smaller the light output. Moreover one has to consider that this compound is characterized by an extremely tiny Light Yield (LY):  $1 \div 2 \text{ keV/MeV}$ .

The purpose of this work is to study the most important parameters (energy resolution,  $\alpha$  vs  $\gamma$  discrimination, internal radiopurity) on a crystal whose size (330 g) matches very closely the requirement of a next generation  $0\nu\text{DBD}$  experiment.

## 2 Experimental set-up

The 330 g  $\text{ZnMoO}_4$  crystal studied in this work was grown in the Nikolaev Institute of Inorganic Chemistry (NIIC, Novosibirsk, Russia). Starting material for the crystal growth were high purity ZnO (produced by Umicore) and  $\text{MoO}_3$ , synthesized by NIIC.

Crystals are grown by the low-thermal-gradient Czochralski technique (LTG Cz) [18] from a melt contained in a 80 mm diameter platinum crucible. The sample was cut from one of the first large-size crystals grown by the LTG Cz. The development of the growth process of  $\text{ZnMoO}_4$  is

at the very beginning, and the shape of the crystal is non-optimal. The final form of the crystal was chosen as a compromise between a large crystal size and the minimization of visible defects. The shape of the crystal sample used in the current work is an irregular polyhedron with 5 sides whose cross section can be roughly assimilated to a  $42 \times 42 \text{ mm}^2$  square. The only parallel faces are the top and bottom ones. All the surfaces are matted, except the one faced to the light detector, that was polished. Unlike previous small samples [19, 20] that were colorless, this crystal shows an uniform orange tint.

The  $\text{ZnMoO}_4$  crystal is held by means of four S-shaped PTFE supports fixed to cylindrical Cu columns: two on the top and two on the bottom. The crystal is surrounded laterally and on the bottom part (with no direct thermal contact) by a plastic reflecting sheet (3M VM2002). The temperature sensors are  $3 \times 3 \times 1 \text{ mm}^3$  Neutron Transmutation Doped (NTD) germanium thermistors, the same used in the Cuoricino experiment. For redundancy we decided to use two thermistors. Each of them is thermally coupled to the crystal via 9 glue spots of  $\approx 0.6 \text{ mm}$  diameter and  $\approx 50 \mu\text{m}$  height.

At the working temperature of our bolometers ( $10 \div 30 \text{ mK}$ ), no “standard” light detectors can work properly. The best way to overcome this problem is to use a second—very sensitive—“dark” bolometer that absorbs the scintillation light giving rise to a measurable increase of its temperature [21]. Our Light Detector (LD) consists of a 50 mm diameter, 260  $\mu\text{m}$  thick pure Ge crystal absorber facing the polished surface of the crystal. A schematic view of our set-up is presented in Fig. 1.

The detectors were operated deep underground in the Gran Sasso National Laboratories in the CUORE R&D test cryostat. The details of the electronics and the cryogenic facility can be found elsewhere [22–24].

The heat and light pulses, produced by a particle interacting in the absorber and transduced in a voltage pulse by the NTD thermistors, are amplified and fed into an 18-bits NI-6284 PXI ADC unit. The trigger is software generated on each thermistor and when it fires 1 s long waveforms, sampled at 2 kHz, are then saved on disk. The time window for the LD is shorter and corresponds to 250 ms. Moreover, when the trigger of a  $\text{ZnMoO}_4$  thermistor fires, the corresponding waveform from the LD is recorded, irrespective of its trigger.

As one of the main goals of the measurements was to test the  $\alpha$  vs  $\beta/\gamma$  discrimination capability of this large crystal, a  $^{238}\text{U}/^{234}\text{U}$   $\alpha$  source was faced to the crystals, on the opposite side with respect to the LD. The source was covered with a 12  $\mu\text{m}$  thick polyethylene film, in order to smear the  $\alpha$ 's energies down to the  $^{100}\text{Mo}$   $Q_{\beta\beta}$ -value. Since mounted close to the detector, this source is responsible for an increase of the  $\alpha$  background that could in principle spoil

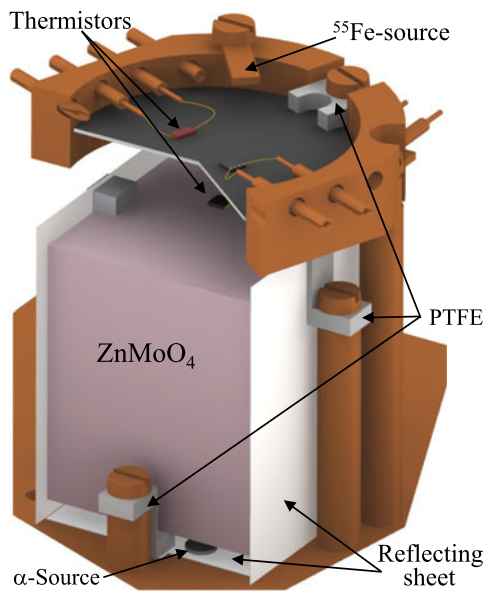


**Fig. 1** Set-up of the detectors. The ball-bonded Au wires are crimped into “male” Cu tubes (pins) and inserted into ground-insulated “female” Cu tubes. Custom wires from detectors towards cryostat are not drawn. A section of the light detector and of the reflecting sheet is not drawn for a better understanding

our sensitivity to the intrinsic contamination of the  $\text{ZnMoO}_4$  crystal. However, the straggling of alpha particles inside the polyethylene film “shifts” the  $^{238}\text{U}/^{234}\text{U}$   $\alpha$ -particles toward lower energies (i.e. below 4 MeV) removing a possible interference with the 4 MeV peak that should appear in the case of a  $^{232}\text{Th}$  bulk contamination of the crystal.

The  $\gamma$  calibration of the  $\text{ZnMoO}_4$  crystal is performed through removable  $^{228}\text{Th}$  and  $^{40}\text{K}$  sources inserted between the dewar housing the cryostat and the external lead shield. The energy calibration of the LD is achieved thanks to a permanent  $^{55}\text{Fe}$  X-ray source, producing two X-rays at 5.9 and 6.5 keV, faced closely to the LD.

### 2.1 Data analysis

The amplitude and the shape of the voltage pulse is determined by the off-line analysis that makes use of the Optimum Filter technique [25, 26]. The signal amplitudes are computed as the maximum of the filtered pulse. The amplitude of the light signal is estimated from the value of the filtered waveform at a fixed time delay with respect to the signal of the  $\text{ZnMoO}_4$  bolometer, as described in detail in Ref. [27]. The signal shape is evaluated on the basis of four different parameters:  $\tau_R$ ,  $\tau_D$ , TVL and TVR.  $\tau_R$  (the rise time) and  $\tau_D$  (the decay time) are evaluated on the raw pulse as  $(t_{90\%}-t_{10\%})$  and  $(t_{30\%}-t_{90\%})$  respectively. TVR (Test Value Right) and TVL (Test Value Left) are computed on the filtered pulse as the least square differences with respect to

**Table 1** Technical details for the  $\text{ZnMoO}_4$  bolometer (Thermistor 1 and Thermistor 2) and for the LD. Signal represents the absolute voltage drop across the thermistor for a unitary energy deposition

Crystal	Signal [ $\mu\text{V}/\text{MeV}$ ]	$\text{FWHM}_{\text{base}}$ [keV]	$\tau_R$ [ms]	$\tau_D$ [ms]
$\text{ZnMoO}_4$ -1	25	3.6	12.8	59.8
$\text{ZnMoO}_4$ -2	23	3.7	12.0	60.3
LD	1800	0.20	3.2	8.2

the filtered response function<sup>1</sup> of the detector: TVR on the right and TVL on the left side of the optimally filtered pulse maximum. These two parameters do not have a direct physical meaning, however they are extremely sensitive (even in noisy conditions) to any difference between the shape of the analyzed pulse and the response function. The detector performances are reported in Table 1. The baseline resolution,  $\text{FWHM}_{\text{base}}$ , is governed by the noise fluctuation at the filter output, and does not depend on the absolute pulse amplitude.

As mentioned above, the use of two thermistors on the same absorber is often made for redundancy. In this case we took advantage of the similar performance of both of them, using their sum. This technique is useful in the case that the noise fluctuations of the two thermistors are not correlated, meaning that these fluctuations are not actual temperature fluctuation of the crystal. This technique can be used in two different ways. One can off-line combine the energies measured by the two thermistors into a “weighted” energy estimator [28], linear combination of the two thermistors. Or, as in this case, one can sum the two signals at hardware level and treat the obtained signal as an additional independent channel. In our case the sum is performed after the two signals are amplified and just before they are fed into the acquisition. The calibration spectrum obtained on the sum of the two thermistors is presented in Fig. 2.

The baseline energy resolution,  $\text{FWHM}_{\text{base}}$  evaluated on the sum ( $\text{ZnMoO}_4$ -Sum) is 2.6 keV, slightly better with respect to the ones reported in Table 1. The FWHM energy resolutions obtained at different energies are reported in Table 2.

### 3 $\alpha$ vs $\beta/\gamma$ discrimination

As described in Sect. 1, the possibility to discriminate the  $\alpha$  interaction results to be the actual key point for a DBD bolometer. As described in details in [19], in scintillating  $\text{ZnMoO}_4$  bolometers the  $\alpha$  vs  $\beta/\gamma$  discrimination can be

<sup>1</sup>The response function of the detector, i.e. the shape of a pulse in absence of noise, is estimated from the average of a large number of raw pulses. It is also used, together with the measured noise power spectrum, to construct the transfer function of the Optimum Filter.

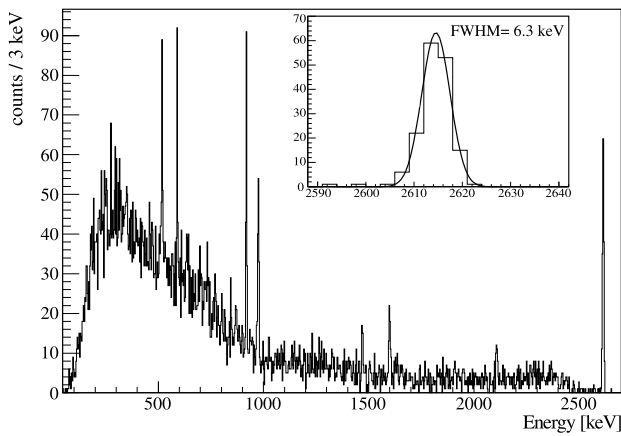


**Fig. 2** Calibration spectrum obtained by exposing the ZnMoO<sub>4</sub> crystal to the <sup>228</sup>Th source for 80 h. The peak at 2615 keV of <sup>208</sup>Tl, magnified in the inset, shows a FWHM resolution of 6.3 keV

**Table 2** FWHM energy resolutions of the ZnMoO<sub>4</sub> detector evaluated on the two thermistors and on their sum

	ZnMoO <sub>4</sub> -1 [keV]	ZnMoO <sub>4</sub> -2 [keV]	ZnMoO <sub>4</sub> -Sum [keV]
583 keV	4.1 ± 0.7	3.0 ± 0.5	2.9 ± 0.4
911 keV	4.9 ± 0.4	4.7 ± 0.5	4.0 ± 0.4
1461 keV	4.9 ± 1.5	5.4 ± 1.2	4.9 ± 1.0
2615 keV	6.8 ± 0.4	6.6 ± 0.6	6.3 ± 0.5

obtained in two different ways: using the light signal and/or by using the PSD. We define discrimination power (DP) between the  $\alpha$  and  $\beta/\gamma$  distributions the difference between the average values of the two distributions normalized to the square root of the quadratic sum of their widths:

$$DP = \frac{\mu_{\beta/\gamma} - \mu_{\alpha}}{\sqrt{\sigma_{\beta/\gamma}^2 + \sigma_{\alpha}^2}} \quad (1)$$

### 3.1 Light vs heat discrimination

The light-to-heat energy ratio<sup>2</sup> as a function of the heat energy is shown for the calibration spectrum in Fig. 3.  $\beta/\gamma$  and  $\alpha$  decays give rise to very clear separate distributions. In the upper band, ascribed to  $\beta/\gamma$  events, the 2615 keV  $\gamma$ -line is well visible. The lower band, populated by  $\alpha$  decays, shows the continuous background induced by the degraded  $\alpha$  source.

The evaluated LY of the ZnMoO<sub>4</sub> crystal is  $1.54 \pm 0.01$  keV/MeV. This value is surprisingly larger (+40 %) with respect to our previous measurements on 30 g (colorless) samples [19]. This, unexpected, larger LY results in

<sup>2</sup>Since we attribute to the heat peaks the nominal energy of the calibration  $\gamma$ 's, the light-to-heat energy ratio also represents the Light Yield of the crystal.

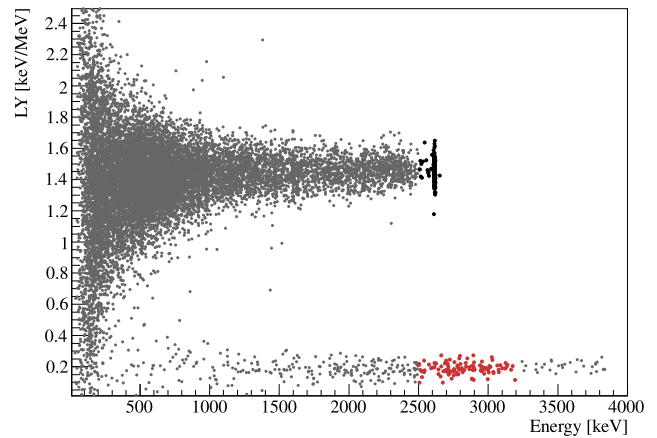


**Fig. 3** The light-to-heat energy ratio as a function of the heat energy obtained in the 80 h <sup>228</sup>Th calibration with ZnMoO<sub>4</sub>-Sum. The *upper band* (ascribed to  $\beta/\gamma$  events) and *lower band* (populated by  $\alpha$  decays) are clearly separated. The 2615 keV <sup>208</sup>Tl  $\gamma$ -line is well visible in the  $\beta/\gamma$  band as well as the continuous background induced by the degraded  $\alpha$  source. The events belonging to the energy region  $2.5 \div 3.2$  MeV (highlighted in the plot) are used to evaluate the DP, that results  $\approx 19$

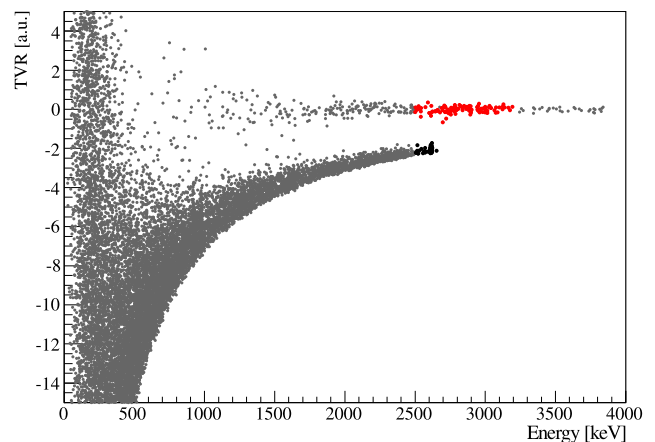


**Fig. 4** TVR as a function of the energy, for the same events of Fig. 3. The *upper band* is populated by  $\alpha$  particles (events in the  $2.5 \div 3.2$  MeV energy range are shown in red) while  $\beta/\gamma$ 's contribute to the lower band (events in the  $2.5 \div 3.2$  MeV energy range are shown in black)

an increase of the DP using the scintillation light. Considering the events in the  $2.5 \div 3.2$  MeV region (see Fig. 3) we estimate a DP of  $\approx 19$ . Moreover the scintillation yield evaluated on the internal  $\alpha$ -line of <sup>210</sup>Po (see Sect. 4) is  $0.257 \pm 0.002$  keV/MeV that corresponds to a scintillation Quenching Factor of  $0.167 \pm 0.002$ . This value is fully compatible with the one ( $0.18 \pm 0.02$ ) obtained on the 30 g sample.

### 3.2 Pulse shape discrimination

The PSD performed in this work is obtained with the same method described in [19]. In Fig. 4 we plot the TVR vari-

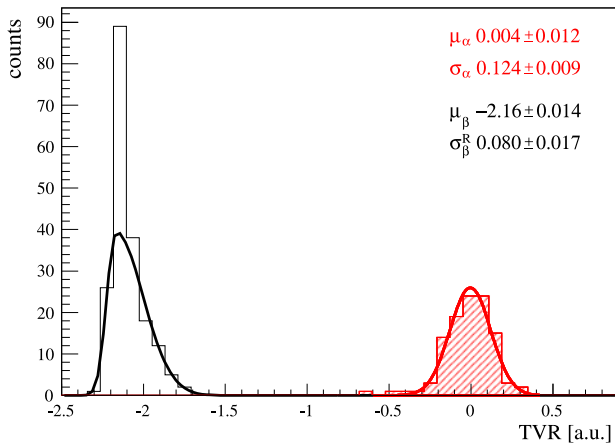


**Fig. 5** TVR histogram of the events of Fig. 4: the  $\alpha$  sample in red and the  $\beta/\gamma$  in black. The mean values and the standard deviations, as estimated from a Gaussian fit, are reported. The  $\beta/\gamma$  distribution was fit with an asymmetric Gaussian. The sigma of the right part of the gaussian ( $\sigma_{\beta}^R$ ) is used to evaluate the DP. From Eq. (1) a discrimination power of  $\approx 14$  is obtained

able as a function of the energy for the same data sample of Fig. 3. As for the case of Fig. 3,  $\beta/\gamma$  and  $\alpha$  events are distinctly separated. The obtained DP with the PSD is  $\approx 14$ , as shown in Fig. 5. It has to be pointed out the “opposite” behaviour of the discrimination power with respect to the results obtained on the 30 g small samples [19] in which we obtained  $\approx 8$  with the light signal and  $\approx 20$  with the PSD. This is due to two distinct mechanisms. First the crystal tested in this work (despite its larger size and orange tint) emits  $\approx 40\%$  more light with respect to the small (colorless) sample previously tested. This implies, obviously, an improved DP of the scintillation light. Second the PSD is sensitive to the S/N ratio. In this work the  $\text{FWHM}_{\text{base}}$  resolution is 4 times worse with respect to the sample previously tested.

#### 4 Internal contaminations

The internal radioactive contaminations of this crystal were evaluated summing up background and different calibration runs for a total collected statistics of 524 h. The corresponding  $\alpha$ -spectrum is presented in Fig. 6. We found a contamination of  $^{226}\text{Ra}$  (it shows a very clear  $\alpha$  and “BiPo” decay pattern sequence). This contamination is evaluated as  $27 \pm 6 \mu\text{Bq/kg}$ . As often happens, we also found a clear internal contamination of  $^{210}\text{Po}$ , corresponding to an activity of  $700 \pm 30 \mu\text{Bq/kg}$ . No other  $\alpha$  lines appear in the spectrum.

In order to evaluate the limits on other potential dangerous nuclei (in particular the  $^{232}\text{Th}$  chain), we evaluated first the flat  $\alpha$  continuum in an energy region in which no peaks are expected ( $3.6 \div 4$  and  $4.35 \div 4.7$  MeV). Then we studied

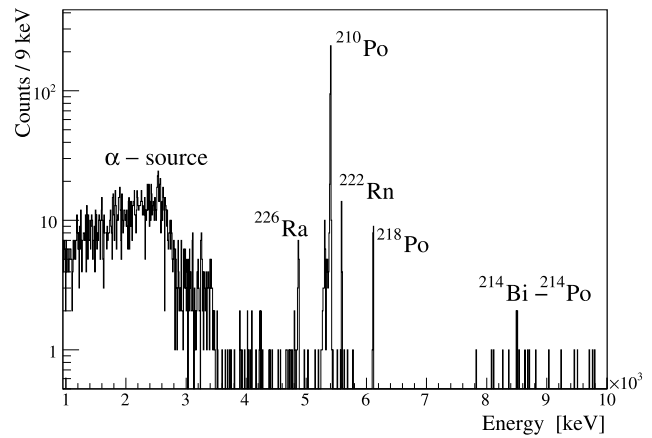


**Fig. 6**  $\alpha$ -spectrum obtained in 524 h of measurement. The contribution of the  $^{238}\text{U}/^{234}\text{U}$   $\alpha$  source is clearly evident below 4 MeV. The internal  $\alpha$ -lines arising from  $^{226}\text{Ra}$  decay chain are highlighted

**Table 3** Evaluated internal radioactive contaminations. Limits are at 90 % CL

Chain	Nuclide	Activity [ $\mu\text{Bq/kg}$ ]
$^{232}\text{Th}$	$^{232}\text{Th}$	$< 8$
	$^{228}\text{Th}$	$< 6$
$^{238}\text{U}$	$^{238}\text{U}$	$< 6$
	$^{234}\text{U}$	$< 11$
	$^{230}\text{Th}$	$< 6$
	$^{226}\text{Ra}$	$27 \pm 6$
	$^{210}\text{Po}$	$700 \pm 30$

an interval of  $\pm 3\sigma$  centered around the Q value of each possible radioactive nucleus, being  $\sigma$  the energy resolution of the  $^{210}\text{Po}$  peak (4.5 keV). The expected flat background contribution in each 27 keV energy window is 0.68 counts. Applying the Feldman-Cousin method [29] using the observed number of counts in each energy window with the expected background, we were able to set 90 % CL limits on several nuclei, as reported in Table 3.

#### 5 Conclusions

For the first time a large mass  $\text{ZnMoO}_4$  crystal was tested as a scintillating bolometer for a possible next generation neutrinoless double beta decay experiment. The bolometer shows an excellent energy resolution. We demonstrated that, even on large mass detector, this compound is able to discriminate  $\alpha$  particles interactions at -practically- any desirable level, using the light information as well as the pulse shape discrimination alone. Moreover this crystal shows an excellent radiopurity.

**Acknowledgements** This work was partially supported by the LUCIFER experiment, funded by ERC under the European Union’s Seventh Framework Programme (FP7/2007-2013)/ERC grant agreement

n. 247115, and by the ISOTTA project, funded within the ASPERA 2nd Common Call for R&D Activities.

Thanks are due to the LNGS mechanical workshop and in particular to E. Tatananni, A. Rotilio, A. Corsi, and B. Romualdi for continuous and constructive help in the overall set-up construction. Finally, we are especially grateful to M. Perego and M. Guetti for their invaluable help.

**Open Access** This article is distributed under the terms of the Creative Commons Attribution Noncommercial License which permits any noncommercial use, distribution, and reproduction in any medium, provided the original author(s) and source are credited.

## References

1. A. Strumia, F. Vissani, [hep-ph/0606054v3](#) (2010)
2. F.T. Avignone III, S.R. Elliott, J. Engel, *Rev. Mod. Phys.* **80**, 481 (2008)
3. W. Rodejohann, *Int. J. Mod. Phys. E* **20**, 1833 (2011)
4. A.S. Barabash, *Phys. Part. Nucl.* **42**, 613 (2011)
5. M. Auger et al., *Phys. Rev. Lett.* **109**, 032505 (2012)
6. A. Gando et al., *Phys. Rev. C* **85**, 045504 (2012)
7. S. Pirro, *Eur. Phys. J.* **27**, 25 (2006)
8. L. Cardani et al., *JINST* **7**, P01020 (2012)
9. E. Andreotti et al., *Astropart. Phys.* **34**, 822 (2011)
10. M. Clemenza et al., *Eur. Phys. J. C* **71**, 1805 (2011)
11. C. Arnaboldi et al., *Nucl. Instrum. Methods A* **518**, 775 (2004)
12. M. Pavan et al., *Eur. Phys. J. A* **36**, 159 (2008)
13. S. Pirro et al., *Phys. At. Nucl.* **69**, 2109 (2006)
14. L. Ivleva et al., *Crystallogr. Rep.* **53**, 1087 (2008)
15. L. Gironi et al., *JINST* **5**, P11007 (2010)
16. C. Arnaboldi et al., *Astropart. Phys.* **34**, 797 (2011)
17. L. Gironi, *J. Low Temp. Phys.* **167**, 504 (2012)
18. E.N. Galashov et al., *Funct. Mater.* **17**, 504 (2010)
19. J.W. Beeman et al., *Astropart. Phys.* **35**, 813 (2012)
20. J.W. Beeman et al., *Phys. Lett. B* **710**, 318 (2012)
21. S. Pirro et al., *Nucl. Instrum. Methods A* **559**, 361 (2006)
22. S. Pirro et al., *Nucl. Instrum. Methods A* **559**, 672 (2006)
23. C. Arnaboldi et al., *Nucl. Instrum. Methods A* **559**, 826 (2006)
24. C. Arnaboldi et al., *Nucl. Instrum. Methods A* **559**, 361 (2006)
25. E. Gatti, P.F. Manfredi, *Riv. Nuovo Cimento* **9**, 1 (1986)
26. V. Radeka, N. Karlovac, *Nucl. Instrum. Methods A* **52**, 86 (1967)
27. G. Piperno, S. Pirro, M. Vignati, *JINST* **6**, P10005 (2011)
28. J.W. Beeman et al., *Astropart. Phys.* **35**, 558 (2012)
29. G. Feldman, R. Cousins, *Phys. Rev. D* **57**, 3873 (1998)